The role of quantum effects and non-equilibrium transport coefficients for relativistic heavy ion collisions

M Berenguer†, C Hartnack†, G Peilert†, H Stöcker†, W Greiner†, J Aichelin‡ and A Rosenhauer§

† Institut für Theoretische Physik, J W Goethe-Universität, D-6000 Frankfurt am Main, Federal Republic of Germany
‡ Institut für Theoretische Physik, Universität Heidelberg, D-6900 Heidelberg, Federal Republic of Germany
§ Department of Physics, University of Bergen, N-5000 Bergen, Norway

Abstract. Stopping power and thermalization in relativistic heavy ion collisions is investigated employing the quantum molecular dynamics approach. For heavy systems stopping of the incoming nuclei is predicted, independent of the energy. The influence of the quantum effects and their increasing importance at low energies, is demonstrated by inspection of the mean free path of the nucleons and the n–n collision number. Classical models, which neglect these effects, overestimate the stopping and the thermalization as well as the collective flow and squeeze out. The sensitivity of the transverse and longitudinal momentum transfer to the in-medium cross section and to the pressure is investigated.

The usefulness of thermodynamic concepts, e.g. density, temperature and pressure, is discussed. Local equilibration can be defined only in a fluid picture. It is proven that the projectile and target nuclei do not penetrate into each other, as assumed in the two-fluid model. They both collide instead with a 'participant' component, which consists of those nucleons which have suffered at least one collision. Local equilibration can reach up to about 80% in each separated fluid.

It is shown that the stress tensor in a one-fluid model cannot be cast in the Newtonian form due to the non-isotropic structure dictated by the initial conditions in relativistic heavy ion collisions. In the 'three-fluid' picture the transverse and longitudinal viscosity coefficients have nearly the same magnitude. Thus, both one- and two-fluid viscous hydrodynamic models are not justified microscopically. The three-fluid model and anisotropic hydrodynamics are currently the only macroscopic models which are supported by the microscopic theory.

1. Motivation

One of the central motivations for studying heavy ion collisions at high energies is the unique opportunity to probe, in the laboratory, hot dense nuclear matter, e.g. the nuclear viscosity and the equation of state. Unfortunately, compression prevails in nuclear collisions only for a very short period and the nucleons continue to interact while the system decompresses. Signatures from the compression stage can be distorted by these final-state interactions. Theoretical studies are needed to find observables linked unambiguously to the densest and most excited state, and are useful for measuring the thermodynamical properties of the system. Furthermore

the concept of the equation of state is based on local equilibrium. It is therefore an important question as to what degree the hot and compressed nuclear matter thermalizes. This question is most important if one wants to use hydrodynamic concepts to describe the dynamics of heavy ion reactions.

Hydrodynamic calculations revealed that the collective transverse flow probes both the viscosity and the compression energy built up in the collision [1–18]. The transverse flow has been experimentally discovered by the GSI/LBL plastic ball and streamer champer groups [19–29]. It arises as a consequence of the build-up of pressure, which causes the release of the compression energy when the system expands. However, the viscosity strongly damps the collective flow. The high temperature achieved in such reactions, as well as the non-equilibrium and momentum-dependent effects due to the highly anisotropic momentum distribution, diminish the sensitivity of the flow observables to the static part of the nuclear potential.

Now the question arises as to how the system evolves from this highly anisotropic initial stage into the final stage. In order to describe the time evolution of such non-equilibrium processes several distinct microscopic models have been developed. The most common ones are the one-body models of the Vlasov–Uehling–Uhlenbeck (VUU)type [30–39] and the molecular dynamic models, which treat the many-body correlations in a purely classical way [40–49]. This latter type of model has been developed further by the inclusion of the most important quantum effects [50–58] and has been widely used to describe the fragmentation process in nuclear collisions.

In-medium effects like the possible reduction of the nucleon–nucleon scattering cross section [59–61] and the momentum dependence of the nucleon–nucleon interactions (MDI) [62] have an influence on the dynamics. Neither the density dependence of the MDI, nor the correction of the cross section in dense and excited nuclear matter are known and therefore it is certainly necessary to investigate how far the results of theoretical calculations are influenced by both effects. The interplay between the in-medium effects and the equation of state (EOS) on nuclear stopping is also studied in this article.

MDI were first implemented in heavy ion collisions in early studies of molecular dynamics [40, 42, 44] as well as in the multiple scattering model [63] and the time-dependent meson field approach [65]. These models predict a significant influence for non-local interactions on the observables: the inclusion of MDI leads to an increase in the collective transverse flow as compared to a local potential alone.

The effective scattering cross section, on the other hand, determines the number of n–n collisions in which the incident kinetic energy is thermalized. The sensitivity of the longitudinal flow to Pauli corrections of the cross sections has recently been demonstrated in VUU [33, 67] as well as in QMD [51, 52] calculations.

These models have successfully described heavy ion reactions on the one-particle level. However, to compare these with experimental data, the fragmentation process must also be described correctly. It has been shown experimentally [25–29] that multi-fragmentation plays a dominant role in this energy regime. The QMD model can indeed describe the dynamics of multi-fragmentation in this energy regime quite well [51–53]. Recently some attempts have been made to incorporate the fragmentation process in the VUU-type models [67–68].

One of the most important problems in such semiclassical microscopic models is the missing antisymmetrization. The Fermi motion has up until now been incorporated by hand into these models (see, however, [69]). Therefore, the fragments produced have some unrealistic properties. In particular, in the true ground state

the nucleons would have vanishing momenta. In 1977 Wilets *et al* [41] had already proposed that this problem could be remedied by simulating the Fermi motion of the nucleons by a quasiclassical momentum-dependent Pauli potential (see also [57, 70]). The inclusion of a Pauli potential strongly influences the EOS at subsaturation densities [71]. It appears necessary to include this effect in the dynamical models [56–58, 71].

Non-equilibrium effects can be taken into account in nuclear fluid dynamics (NFD) by means of the viscosity and heat conduction terms, if one assumes that the deviations from local equilibrium are small. Elementary kinetic theory [72–74] connects the viscosity coefficient η and the effective scattering cross section σ^{eff} via the relation $\eta \propto 1/\sigma^{\text{eff}}$, hence the size of η directly influences the amount of nuclear stopping. It has been shown [76] that the nuclear viscosity strongly decreases the transverse flow by a factor of roughly two if η is increased from zero (ideal fluid) to $\eta = 60$ MeV fm^{-2} c^{-1}.

In viscous hydrodynamics a viscosity coefficient of this size is needed in order to match the calculated transverse flow with the data. Values of this order of magnitude have been derived for hot, infinite nuclear matter from the classical kinetic theory [72] and in the Uhlenbeck–Uehling equation [73] and have also been obtained by means of fluid dynamic scaling analysis [63, 64].

2. The QMD model

The QMD approach, which is described in detail in [51–53], incorporates the important quantum features of the VUU theory [30–39], namely the Pauli principle, stochastic scattering and particle production, into the N-body phase space dynamics of the classical molecular dynamics method [40–48].

The nucleons are represented by Gaussians of the form

$$f_i(r, p, t) = \frac{1}{(\pi\hbar)^3} \exp\left\{-\frac{(r - r_{i0}(t))^2}{2L} - (p - p_{i0}(t))^2 \frac{2L}{\hbar^2}\right\} \qquad (1)$$

where r_{i0} and p_{i0} are the centroids of particle i in coordinate and momentum space.

The phase space distribution can now be expressed as

$$f(r, p, t) = \sum_{i=1}^{N} f_i(r, p, t). \qquad (2)$$

In terms of these Gaussians the baryon density is given by

$$\varrho_B(r, t) = \sum_{i=1}^{N} \int f_i(r, p, t)\, \mathrm{d}^3 p = \frac{1}{(2\pi L)^{3/2}} \sum_{i=1}^{N} \exp[-(r - r_{i0})^2/2L]. \qquad (3)$$

With the knowledge of the phase space distribution it is possible to calculate thermodynamical quantities locally. The ensemble average of a macroscopic quantity $\chi(r, t)$ is given by

$$\langle \chi(r, t)\rangle = \frac{1}{\rho(r, t)} \int \mathrm{d}^3 p \, \chi(p, r, t) f(p, r, t). \qquad (4)$$

The interactions used here are a local Skyrme two- and three-particle interaction, a Coulomb and a Yukawa interaction. In some cases we also include a MDI which has been adapted from the experimental values of the real part of the proton–nucleus optical potential.

With those Gaussian nucleons, our interactions lead to the following Hamiltonian:

$$
\begin{aligned}
H = \sum_{i=1}^{N} \frac{p_i^2}{2m} + \frac{1}{2} \sum_{i,j=1}^{N} {}' \int f_i(r_i, p_i, t) V_{Yuk}^0 \\
\times \frac{\exp(-|r_i - r_j|/\gamma_{Yuk})}{|r_i - r_j|} f_j(r_j, p_j, t) \, dr_i \, dr_j \, dp_i \, dp_j \\
+ \left(\frac{Z}{A}\right)^2 \frac{1}{2} \sum_{i,j=1}^{N} {}' \int f_i(r_i, p_i, t) \frac{e^2}{|r_i - r_j|} f_j(r_j, p_j, t) \, dr_i \, dr_j \, dp_i \, dp_j \\
+ \frac{1}{2} \sum_{i,j=1}^{N} {}' \int f_i(r_i, p_i, t) \alpha \delta(r_i - r_j) f_j(r_j, p_j, t) \, dr_i \, dr_j \, dp_i \, dp_j \\
+ \frac{1}{6} \sum_{i,j,k=1}^{N} {}' \int f_i(r_i, p_i, t) f_j(r_j, p_j, t) f_k(r_k, p_k, t) \\
\times \beta \delta(r_i - r_j) \delta(r_i - r_k) \, dr_i \, dr_j \, dr_k \, dp_i \, dp_j \, dp_k \\
+ \left(\frac{1}{2} \sum_{i,j=1}^{N} {}' \int f_i(r_i, p_i, t) \delta \ln^2(\epsilon|p_i - p_j|^2 + 1) \right. \\
\left. \times \delta(r_i - r_j) f_j(r_j, p_j, t) \, dr_i \, dr_j \, dp_i \, dp_j \right).
\end{aligned}
\tag{5}
$$

The evaluation of the integrals yields

$$
\begin{aligned}
H = \sum_{i=1}^{N} \frac{p_i^2}{2m} + \frac{1}{2} \sum_{i,j=1}^{N} {}' \frac{V_{Yuk}^0}{2|r_i - r_j|} \exp(L/\gamma_{Yuk}^2) \\
\times \left\{ \exp(-|r_i - r_j|/\gamma_{Yuk}) \left[1 - \mathrm{erf}\left(\frac{(2L/\gamma_{Yuk}) - |r_i - r_j|}{\sqrt{4L}} \right) \right] \right. \\
\left. - \exp(+|r_i - r_j|/\gamma_{Yuk}) \left[1 - \mathrm{erf}\left(\frac{(2L/\gamma_{Yuk}) + |r_i - r_j|}{\sqrt{4L}} \right) \right] \right\} \\
+ \left(\frac{Z}{A}\right)^2 \frac{1}{2} \sum_{i,j=1}^{N} {}' \frac{e^2}{|r_i - r_j|} \mathrm{erf}\left(\frac{|r_i - r_j|}{\sqrt{4L}} \right) \\
+ \sum_{i=1}^{N} \left[\frac{\alpha}{2} \frac{1}{(4\pi L)^{3/2} \varrho_0} \sum_{j=1}^{N} {}' \exp\left(-\frac{(r_{i0} - r_{j0})^2}{4L} \right) \right. \\
\left. + \frac{\beta}{\gamma + 1} \left(\frac{1}{(4\pi L)^{3/2} \varrho_0} \sum_{j=1}^{N} {}' \exp\left(-\frac{(r_{i0} - r_{j0})^2}{4L} \right) \right)^{\gamma} \right]
\end{aligned}
$$

$$+ \sum_{i=1}^{N} \left[\delta \ln^2 (\epsilon |p_{i0} - p_{j0}|^2 + 1) \frac{1}{(4\pi L)^{3/2} \varrho_0} \right.$$

$$\left. \times \sum_{j=1}^{N}{}' \exp \left(-\frac{(r_{i0} - r_{j0})^2}{4L} \right) \right]. \tag{6}$$

The primes on the sums indicate that the self-interaction terms are omitted. The three-body part of the Skyrme interaction is here approximated to be proportional to ϱ^γ, in order to allow the compressibility of nuclear matter to be varied as well.

The parameters α, β and γ are adjusted to reproduce the properties of infinite nuclear matter, i.e.

$$\left. \frac{E}{A} \right|_{\varrho = \varrho_0} = -16 \text{ MeV}$$

$$P = \varrho^2 \left. \frac{\partial E/A}{\partial \varrho} \right|_{\varrho = \varrho_0} = 0 \text{ MeV fm}^3 \tag{7}$$

$$K = 9\varrho^2 \left. \frac{\partial^2 E/A}{\partial \varrho^2} \right|_{\varrho = \varrho_0} = \begin{cases} 200 \text{ MeV} & \text{(soft EOS)} \\ 380 \text{ MeV} & \text{(hard EOS).} \end{cases}$$

The parameters of the model are listed in table 1.

Table 1. Parameters of the model for the different interactions.

K (MeV)	EOS	α (MeV)	β (MeV)	γ	δ (MeV)	ϵ (MeV^{-2})	V_{Yuk}^0 (MeV)	γ_{Yuk} (fm)
380	H	−124	70.5	2.0	—	—	−10	1.5
200	S	−356	303	7/6	—	—	−10	1.5
200	SM	−390	320	8/7	1.57	21.54	−10	1.5

The short-range interaction is taken into account in the same way as in the cascade and VUU models via a stochastic scattering term: two nucleons can scatter if the spatial distance of the centroids of their Gaussians is smaller than $\sqrt{\sigma_{tot}/\pi}$. The energy and angular dependence of the experimental differential n–n cross sections $d\sigma/d\Omega$ are reproduced. The free n–n cross sections are modified in a medium by the Uehling–Uhlenbeck blocking factors $[1 - f(r,p)]$ [76], which determine the Pauli blocking probability of the final states in an n–n collision. Inelastic processes have also been implemented [30, 55].

3. The importance of the collision term

Before we investigate the influence of the quantum effects on the reaction dynamics we start with a survey of the time evolution for the reaction Au ($b = 0$ fm) + Au
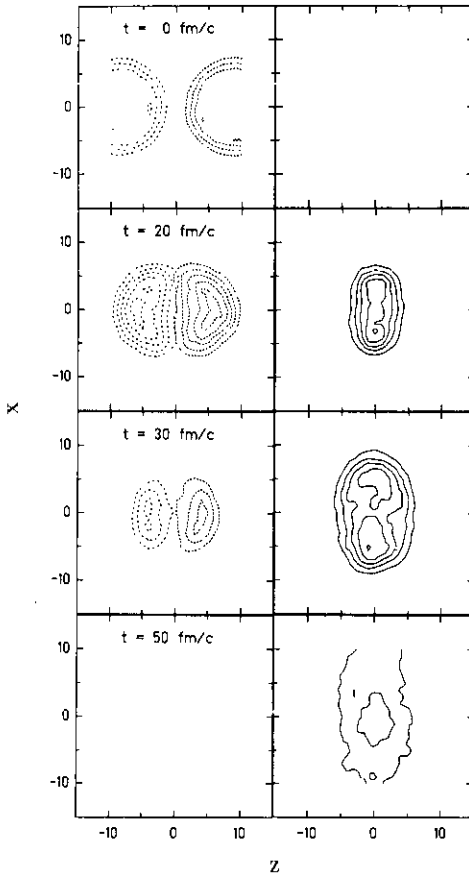
Figure 1. Time evolution of the density contours of the system ^{197}Au (200 MeV/nucleon, $b = 0$ fm) + ^{197}Au for target and projectile nucleons which have not yet collided (left) and for the 'participant' component (right), which includes all particles which have collided at least once. The contour lines are at $\varrho = 0.25, 0.5, 0.75, 1.0, 1.25, 1.5, 1.75, 2\varrho_0$. Note that the spectator fluid barely interpenetrates, but instead collides with the participant nucleons piled up in an ellipsoid at midrapidity.
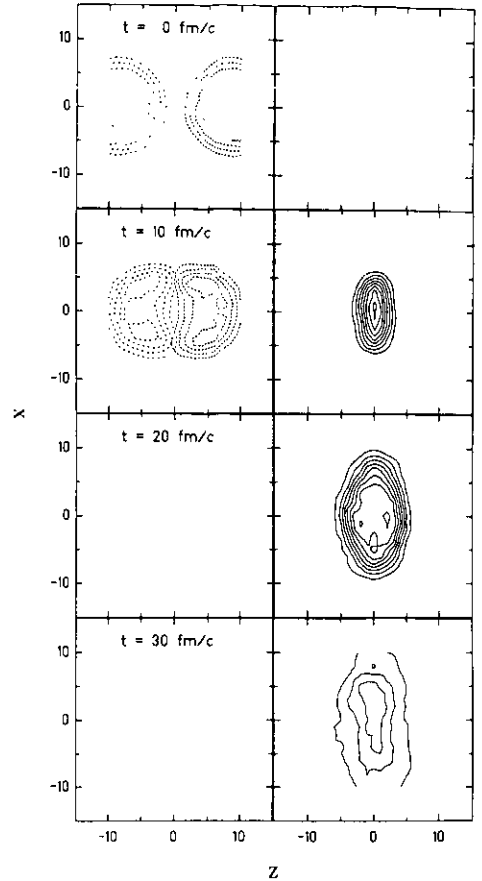
Figure 2. As in figure 1 for the reaction ^{197}Au (800 MeV/nucleon, $b = 0$ fm) + ^{197}Au. At this energy there is no interpenetration of projectile and target.

at 200 and 800 MeV/nucleon bombarding energy. In the following we will define all nucleons which suffered at least one collision as participants.

Figures 1 and 2 show the density profiles of the (cold) projectile and target component in the left-hand column, i.e. all particles that did not collide up to this time. The right-hand column shows the corresponding profiles of the participant component.

It is only at the very beginning of the reaction that there is an overlap between the projectile and target component. The very first collisions (cf figure 8) rapidly build up the participant components. Once these participant components have been

formed, they act as a buffer between target and projectile—they no longer interact directly. The future evolution of the system is completely determined by the separate interaction of the participant matter with the projectile or target, respectively. Interactions within the participant matter are also crucial. This behaviour is in complete contradiction to the two-fluid model [4, 13, 14, 16, 17], where one assumes that the projectile and target component stream through each other and collectively decelerate.
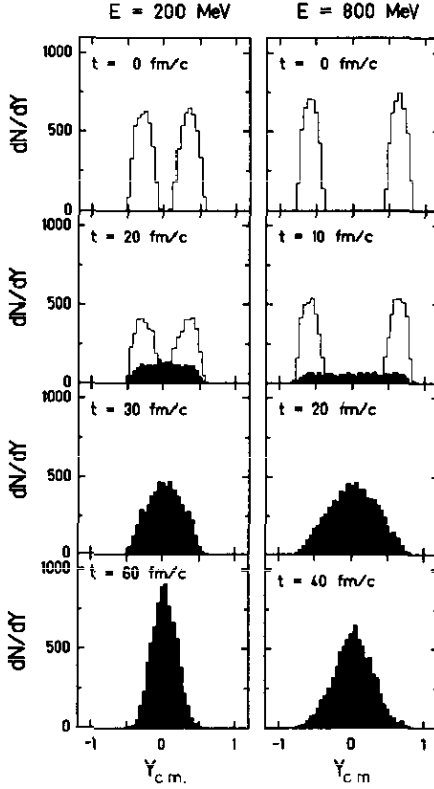

Figure 3. Rapidity distribution dN/dY of the participants (black area) and the spectators (white area) at different reaction times as indicated in central collisions of ^{197}Au (200 (left), 800 (right) MeV/nucleon, $b = 0$ fm) + ^{197}Au. Note that the participants can be distinguished experimentally from the spectators by their rapidities.

The same fact can be observed in momentum space: The dN/dY distribution of the three components is depicted in figure 3. Remnants of the projectile and target do not survive the reaction for $b = 0$ fm. The matter is stopped at the centre of mass rapidity. This supports the three-fluid picture [9, 15].

3.1. The influence of the quantum effects

The influence of the quantum effects can be studied here by comparing the calculations using the free n–n cross section σ^{free} (without Pauli blocking) to the results including the Uehling–Uhlenbeck scattering cross section [76].

$$\sigma^{UU} = \sigma^{\text{free}}(p_1, p_2, p_1', p_2')[1 - f(r, p_1')][1 - f(r, p_2')]. \tag{8}$$

σ^{UU} takes into account the Pauli blocking of the final states of two scattered nucleons. The Pauli blocking factors $[1 - f(r,p)]$ effectively cause a reduction in the free cross section in the medium. This in turn results in a decrease in the number of collisions.

3.2. The mean free path

The influence of this quantum effect on the dynamics of the reaction can most clearly be seen by inspection of the mean free path of the nucleons. The time evolution of all nucleons can be followed in the QMD model. Thus we can 'measure' microscopically the mean free path of all nucleons.
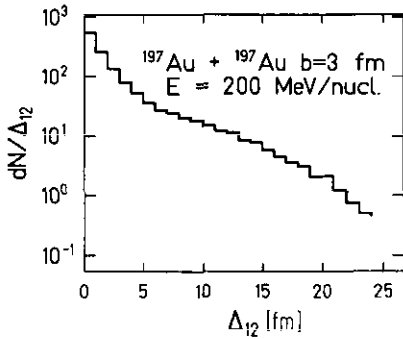
Figure 4. Distribution of the free paths of the nucleons for the reaction ^{197}Au (200 MeV/nucleon, $b = 3$ fm) + ^{197}Au. A large number of nucleons travel only 1–2 fm/c between two collisions. This raises doubts as to whether the dilute gas limit is justified.

Figure 5. The mean free path of the nucleons is shown for the very central Au + Au collisions at energies from 200 to 800 MeV/nucleon (L) $b = 0$ fm for the different n–n cross sections, masses and energies as indicated. Note that λ does not depend on the mass of the system and decreases with increasing bombarding energy in contrast to the naive expectation of classical kinetic theories [74].

In figure 4 the distribution of the 'free path' Δ_{12} of the nucleons between subsequent collisions is depicted. One observes a large number of nucleons which travel only 1 or 2 fm c^{-1} between two collisions. There is a small number of nucleons with $\Delta_{12} > 10$ fm c^{-1}. This raises doubts as to whether the dilute gas limit, which is the main assumption of all transport models, and the neglect of three-body collisions is justified.
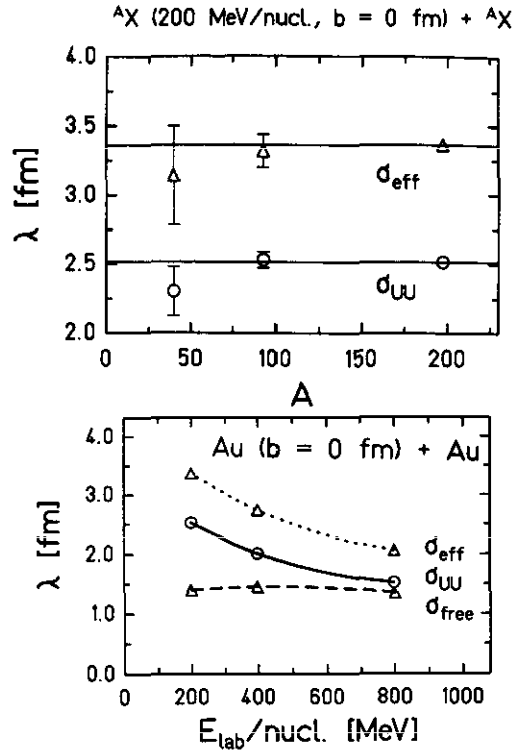
Figure 5 (top) shows the dependence of the mean free path on the mass of the system for central, symmetric reactions. Note that the mean free path λ is defined as the average of the distribution of figure 4, taken over all collisions. The results are shown for the Uehling–Uhlenbeck cross section σ^{UU} and for a reduced cross section σ^{eff}. Here an overall reduction of 30%, as proposed by Malfliet, Batemans and ter Haar [59, 60], has been used in order to take the Pauli blocking of the intermediate scattering states into account. This reduction of the cross section clearly reduces the number of collisions and therefore increases λ. Note that λ depends on the n–n cross section and *not* on the mass of the system. The energy dependence of λ can be studied for the most central collisions of Au on Au in figure 5 (bottom).

λ decreases with increasing bombarding energy, due to the higher densities achieved, in spite of a decreasing n–n cross section. The results obtained with the Boltzmann cross section σ^{free} (without Pauli blocking) is also shown. This increased cross section yields a drastic decrease of the mean free path. Enhanced thermalization and nuclear stopping results.
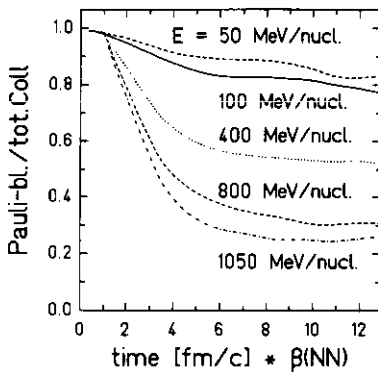

Figure 6. Time dependence of the ratio of Pauli blocked collisions to the total number of attempted collisions at different beam energies for the system ^{93}Nb ($b = 3$ fm) + ^{93}Nb, soft EOS. Observe that Pauli blocking is crucial even for the highest bombarding energies.
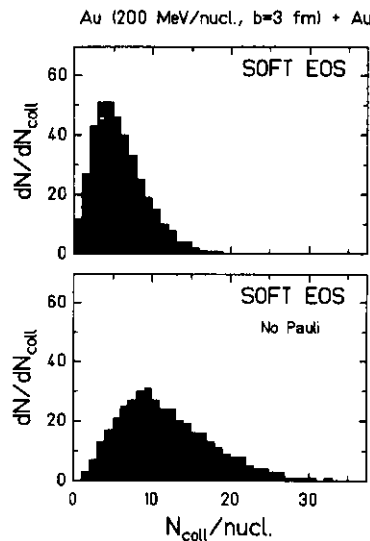
Figure 7. The distribution of the number of collisions is shown for the reaction ^{197}Au (200 MeV/nucleon, $b = 3$ fm) + ^{197}Au for the soft EOS with and without Pauli blocking of the final scattering states.

In order to demonstrate the importance of the Pauli blocking, the fraction of the Pauli blocked collisions to all attempted collisions is shown in figure 6 for the system Nb + Nb for different beam energies between 50 and 1050 MeV/nucleon The ratio is plotted against $t\beta$. Here $t\beta$ is the scaled reaction time, i.e. t multiplied with the velocity β of the incoming projectile in the equal speed system. This product corresponds to the distance travelled by the projectile and target in the z-direction. It scales the time according to the velocity of the incoming projectile.

All curves start with a blocking fraction of one. This is due to the fact that all collisions are Pauli blocked in the ground state. After the two nuclei touch each other the blocking factors decrease and saturate after $t\beta \approx 5$–6 fm. This distance

corresponds to the total overlap of both nuclei. For very low bombarding energies (the TDHF regime) the blocking factor remains close to one, whereas for higher energies it decreases down to 0.2 at 1 GeV/nucleon.

The distribution of the number of n–n collisions is shown in figure 7 for the reaction Au (200 MeV/nucleon, $b = 3$ fm) + Au. This distribution is peaked at about five collisions per nucleon for the soft EOS. The tail, however, shows particles with more than 10–15 collisions. A considerable number of particles have suffered no collisions at all and can therefore be called true spectators. They reside in the nuclear coronas (pole-caps) in these off-centre collisions.

The importance of the quantum effects for the number of collisions is studied in figure 7 (bottom): Without the Pauli blocking the number of collisions doubles and the number of spectators decreases to zero.

Therefore classical molecular dynamic models [40–49], which neglect this quantum effect, overestimate drastically the importance of the n–n collisions, especially at low energies.
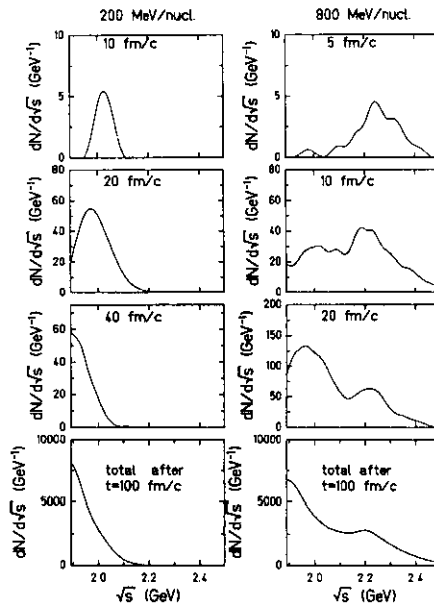

Figure 8. Time dependence of the energy distributions $dN/d\sqrt{s}$ of the n–n collisions in the reactions ^{197}Au (200 and 800 MeV/nucleon, $b = 3$ fm) + ^{197}Au. The beginning of the reaction is clearly governed by hard collisions, while soft collisions dominate further on.

Figure 8 shows the CM energy distributions $dN/d\sqrt{s}$ of the nn collisions, again for the reactions Au (200, 800 MeV/nucleon, $b = 3$ fm) + Au. The lower row give the total, time integrated, distributions. A peak in the energy distribution is due to the first collisions, which occur roughly at the energy $\sqrt{s} = 2m + E_{cm}^{kin}$. This underlines the importance of the non-equilibrium effects at the early times.

The time evolution of the scattering process shows that, while the dynamics in the beginning of the reaction is dominated by high energy collisions, the soft collisions dominate subsequently. Therefore, processes which are most sensitive to the hard collisions, such as (subthreshold) particle production (π, η, K), are mostly influenced by

the initial projectile and target momentum distribution in the early, non-equilibrium stage of the reaction. The collective flow builds up later, when the system is equilibrated and yields the expansion of the system.

3.3. The sensitivity of nuclear stopping to the in-medium cross sections

Let us now inspect in more detail the stopping of the incoming matter which implies the equilibration of the incident longitudinal momenta in n–n collisions.
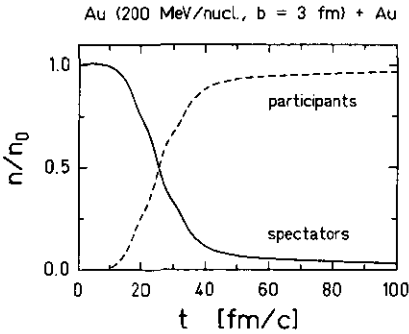
Figure 9. Conversion of the spectators into the participant (fireball) component as a function of time for the same system as in figure 4. All particles having suffered at least one n–n collision are assumed to belong to the fireball component. n/n_0 denotes the ratio of nucleons which belong to the spectator (participant) component. Note the rapid onset of the thermalization process as soon as the nuclei touch each other.
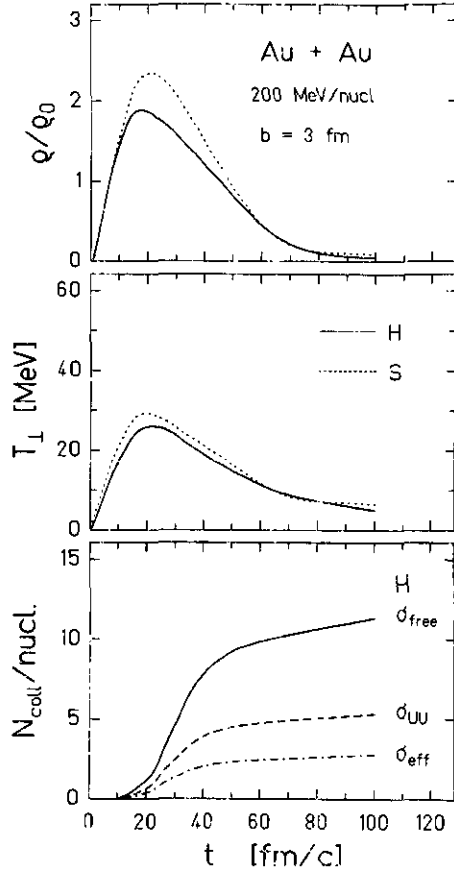
Figure 10. Time evolution of the central compression, the transverse 'temperature' and the average number of collisions per nucleon of the reaction ^{197}Au (200 MeV/nucleon, $b = 3$ fm) + ^{197}Au. The local 'temperature' has been obtained via the relation $T = \langle p_\perp^2 \rangle / 2m$ for the different interactions as indicated. Almost all collisions take place when the 'temperature' and densities are at their highest values.

The thermalization process is associated with the conversion of the cold projectile and target matter into the hot participant (fireball) component. The time evolution of this process is depicted in figure 9 for a central collision. Observe the rapid onset of

the thermalization process, as soon as the nuclei overlap in configuration space. Late in the compression stage almost all nucleons are found in the participant component. This is due to the large number of n–n collisions in the system.

Some quantities of interest for macroscopic models are shown in figure 10 for the reaction Au (200 MeV/nucleon, $b = 3$ fm) + Au as a function of time. The central density increases from zero (in the initial stage the nuclei are separated in coordinate space) to the maximum density reached after 15 fm c^{-1}. The maximum densities achieved in this energy regime are between two and three times normal nuclear matter density depending on the EOS used (with a soft EOS higher densities are reached). After this compression stage the matter flows out of the central region. Therefore the central density decreases steadily to zero.

The same behaviour can be observed in figure 10 (middle) for the transverse kinetic 'temperature', which is defined as $T_\perp = (\langle p_x^2 \rangle + \langle p_y^2 \rangle)/(2m)$.

Hard n–n collisions lead to the degradation of the longitudinal momenta into transverse degrees of freedom, to the build-up of the compression zone and to the complete stopping of the system (figure 10 (bottom)). The average number of n–n collisions per nucleon is plotted as a function of time for different n–n cross sections. Almost all collisions take place in the time interval when the 'temperature' and the density are at their highest values. At the end of the compression stage ($t \approx 50$–60 fm c^{-1}), practically all collisions have ceased. Hence, the following expansion and fragmentation stage is little affected by short-range interactions and the system evolves almost isentropically, although there are still a few collisions occurring within the formed fragments.

The large average collision numbers $N_{\text{coll}}/A \approx 5$ indicate the approach to local equilibrium. Kinetic models predict the thermalization of the incident momenta after only two or three collisions, depending on the beam energy [77–79].

In momentum space equilibration can be characterized by the transition of two initially separated Fermi spheres at $T = 0$ to a thermalized matter distribution at rest in the CM frame.

The final rapidity spectra dN/dY for central and peripheral collisions are shown in figure 11 for the reaction Au (200 MeV/nucleon) + Au. In central collisions complete stopping results in a Gaussian-shaped rapidity distribution at rest in the CM frame. No remnants of the initial rapidity distributions centred around $y = \pm y_{\text{beam}}$ are left. Only a small fraction of the nucleons are stopped and suffer sufficient collisions to thermalize their initial momenta at large impact parameters ($b = 7$ fm). Two broad distributions, centred close to the initial rapidities of target and projectile, represent the spectator residues. They move on with little interaction. The rapidity spectra depend little on the EOS used.

The dependence of the dN/dY distributions on the mass of the system and on the bombarding energy is shown in figure 12: Complete stopping is observed only for massive systems, while lighter systems exhibit broad rapidity distributions even for very central collisions. The stopping power does not change much with bombarding energy, if the scaled rapidity distribution $dN/d(Y/Y_P)$ is considered†.

For the comparison with the plastic ball data [28] we applied an experimental

---

† This, in fact, remains true even for ultra-relativistic energies: The scaled baryon rapidity distributions for lighter systems (Si + Si at 15 GeV/nucleon and S + S at 200 GeV/nucleon) do indeed show the same plateau shape as observed here (for Ne and Ca), both theoretically [84] and experimentally [86, 87]. Also interesting is the theoretical observation that a remarkable part of the baryons is pushed to the mid-rapidity zone at energies up to 0.8 TeV/nucleon [85].
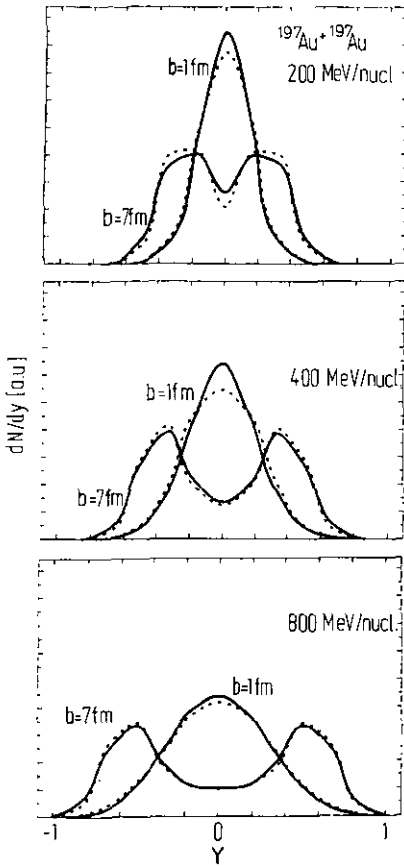
Figure 11. Rapidity distributions for the system ^{197}Au (200 (top), 400 (middle) and 800 (bottom) MeV/nucleon, $b = 1, 7$ fm) + ^{197}Au for a hard (H) and a soft (S) EOS. Note that the rapidity distributions do not depend on the EOS.
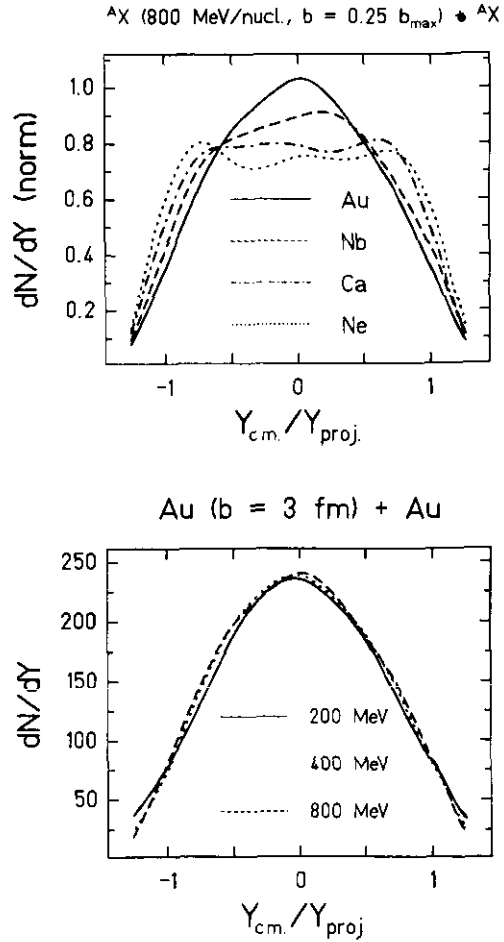
Figure 12. Mass (top) and energy (bottom) dependence of the rapidity distributions for the indicated systems. Complete stopping is observed only for massive systems at all energies investigated.

efficiency filter. Only emitted protons with an energy $E > 25$ MeV and emission angles between $2.5°$ and $160°$ are plotted in the calculated distributions. Figure 13 shows the QMD calculations (right-hand column) compared with the plastic ball data (left-hand column) for different systems at 400 MeV/nucleon. The protons have been determined with a spanning tree cluster algorithm [32, 51, 52]. The shape of the distributions seems to be identical for all systems. However, this insensitivity is only due to the selection of protons (light clusters are predominantly seen at the projectile and target rapidities [51]). For the smaller systems there is more transparency, because the ratio of the mean free path to the diameter of the system is not small enough. The filter furthermore cuts out those particles which remain at target and projectile rapidities, because of their low energy and small angles in the
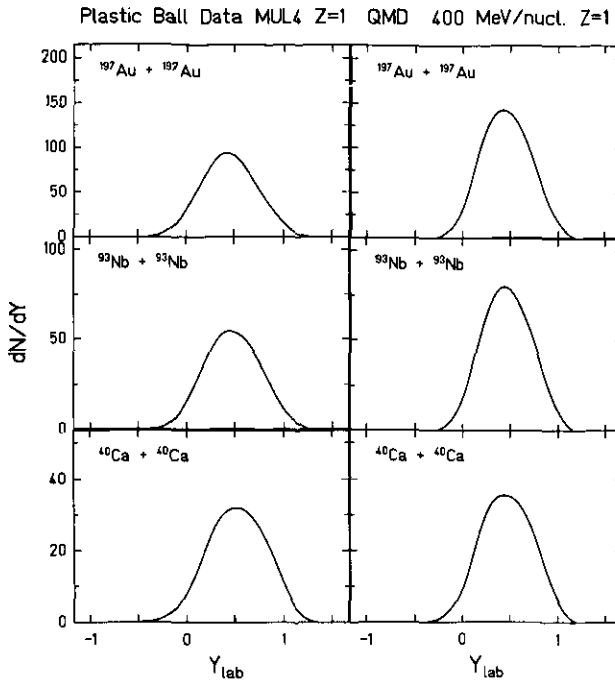
Plastic Ball Data MUL4 Z=1   QMD   400 MeV/nucl. Z=1

Figure 13. Mass dependence of the proton rapidity distributions. The QMD results (right) are compared with the plastic ball data (left). Due to the efficiency cuts of the plastic ball filter all distributions (even those for the light systems) look Gaussian-shaped (see, however, figure 12).

laboratory frame respectively. Thus the plateau shapes of the unfiltered distributions only appear to be Gaussian-shaped because of the efficiency cuts. Non-negligible distortions of the mid-rapidity yields have been reported for the very heavy sytem by the plastic ball collaboration [22–29]. They are due to enhanced double-hit and cross-talk probabilities in this high track density environment. Only detector systems of even higher granularity, e.g. the GSI 4π detector system, can avoid these problems.

The sensitivity of the nuclear stopping to the potential employed and to the effective scattering cross section has also been investigated. Figure 14 shows that the influence of the mean field on the longitudinal flow is relatively small. However, the scattering cross section is vital for the stopping power. By using the free cross section (without Pauli blocking) the classical collision numbers double. This yields an increase in the stopping power. A global reduction of the scattering cross section with $\sigma^{\text{eff}} = 0.7\sigma^{\text{UU}}$ (SIM) yields double peaked dN/dY distributions with peaks closer to the rapidities of the projectile and target. The double peak structure originates from the remnants of the projectile and target spectators. It indicates an incomplete stopping of the incident nuclei. One should, however, keep in mind that a more complex functional dependence of σ^{eff}, e.g. on ρ and T, could render the systematics of the interplay between the effective scattering cross section and the longitudinal and transverse flow much more complicated. The dN/dY distribution of the soft EOS with the Uehling–Uhlenbeck cross section σ^{UU} (S) lies between the curves S and SIM. The MDI (SM) modifies the stopping power slightly. The evident differences between
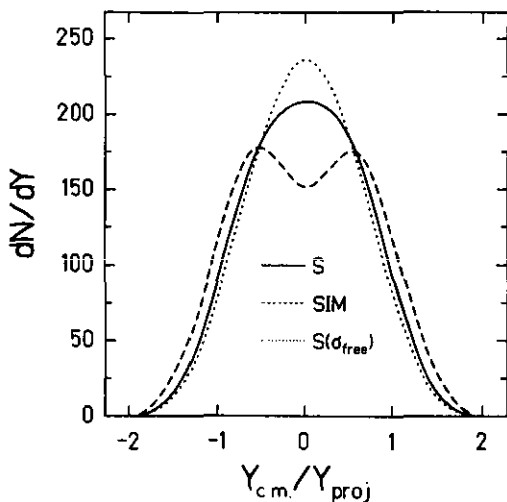
Figure 14. The influence of the different interactions on the rapidity distributions dN/dY (all particles included) obtained from the reaction ^{197}Au (200 MeV/nucleon, $b = 3$ fm) + ^{197}Au. The dN/dY distributions depend strongly on the n–n cross sections used!

the dN/dY spectra obtained from the cases σ^{eff} and σ^{UU} can be exploited for the experimental determination of σ^{eff} from the dN/dY spectra for different systems at different energies (see, e.g., [51, 66]).

The measured rapidity spectra for the systems Ar (1200 MeV/nucleon) + BaI$_2$ and KCl are in good agreement with VUU calculations [67], which use the free scattering cross section σ^{UU}. A reduced—or increased—σ^{eff} fails to reproduce these data, just as the Au + Au data show no dip.

3.4. Transverse momentum transfer and the concept of a temperature'

The interplay between the longitudinal and the transverse flow can be seen clearly by inspection of the double differential cross section $d^2N/dy\,dp_\perp$ in figure 15. It is shown for different impact parameters for the reaction Au (650 MeV/nucleon) + Au.

The final nucleon distribution is centred around the original beam and target rapidities and momenta for peripheral collisions (at $b = 7$ fm). With decreasing impact parameter the two peaks come closer to each other, merge at $b = 3$ fm and form a single 'equilibrated' source for central collisions ($b = 1$ fm). The stopping of the incoming matter is closely related to the transverse momentum transfer. The transverse momenta increase with decreasing impact parameter, indicating the thermalization of the initial beam momenta (The 'thermalization' is studied quantitively in the next section.)

The absolute width of the final momentum distribution is shown in figure 16, where we compare the longitudinal and transverse 'temperatures' of the global system, defined by $T_\perp = (\langle p_x^2 \rangle + \langle p_y^2 \rangle)/2m$ and $T_\parallel = \langle p_z^2 \rangle/m$.

Figure 16 (top and middle) shows the change of the relative magnitude of the longitudinal and the transverse temperature when the impact parameter changes from 1 to 3 fm c^{-1}. Here a hard EOS is used, for the soft EOS the two components of the temperatures are identical. This demonstrates a substantial sensitivity of the directed sidewards flow to the potential (EOS). The transverse flow is less pronounced for the

soft EOS, in agreement with the results obtained with the VUU approach [30, 33]. However, this result does not give sufficient information to conclude that the system is equilibrated, as we will discuss in the next section.
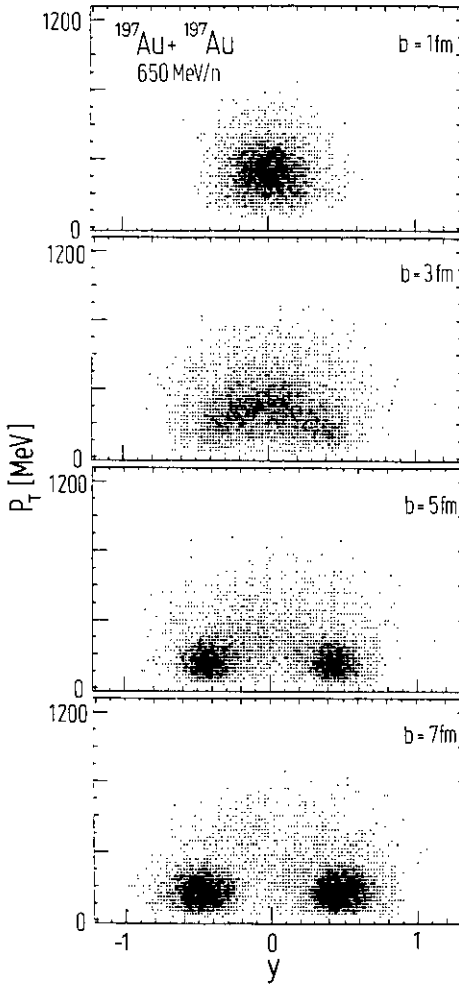

Figure 15. Invariant double differential momentum distribution $d^2 N/dy dp_\perp$ for the reaction ^{197}Au (800 MeV/nucleon, hard EOS) + ^{197}Au at different impact parameters as indicated.
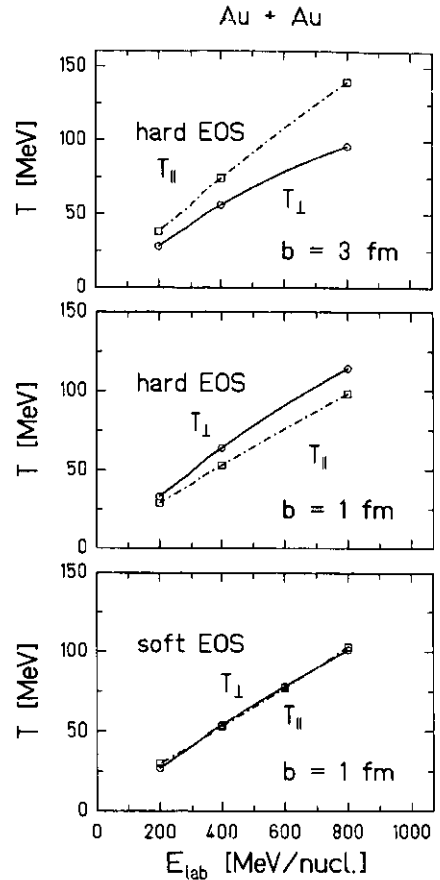
Figure 16. Excitation function of the apparent 'temperatures' in the system ^{197}Au ($b = 1$ and 3 fm) + ^{197}Au. The mean quadratic momenta in beam direction $T_\parallel$ (broken curves) and in transverse direction $T_\perp$ (full curves) are displayed for a hard (top and middle) and a soft (bottom) EOS, respectively in almost central collisions. These 'temperatures' are determined via the corresponding mean quadratic momenta in the CM frame: $T_\parallel = (1/m)\langle p_z^2\rangle$, $T_\perp = (1/2m)[\langle p_x^2\rangle + \langle p_y^2\rangle]$. Note the substantial sensitivity of the directed sidewards flow on the EOS and the impact parameter.

4. The importance of non-equilibrium effects and the transport coefficients

4.1. The pressure and equilibration process

Let us now investigate to what extent thermodynamic concepts, in particular local equilibrium, are justified. The local equilibrium concept forms the basis of ideal fluid dynamics. The assumption of *global equilibrium* forms the basis of most statistical models.
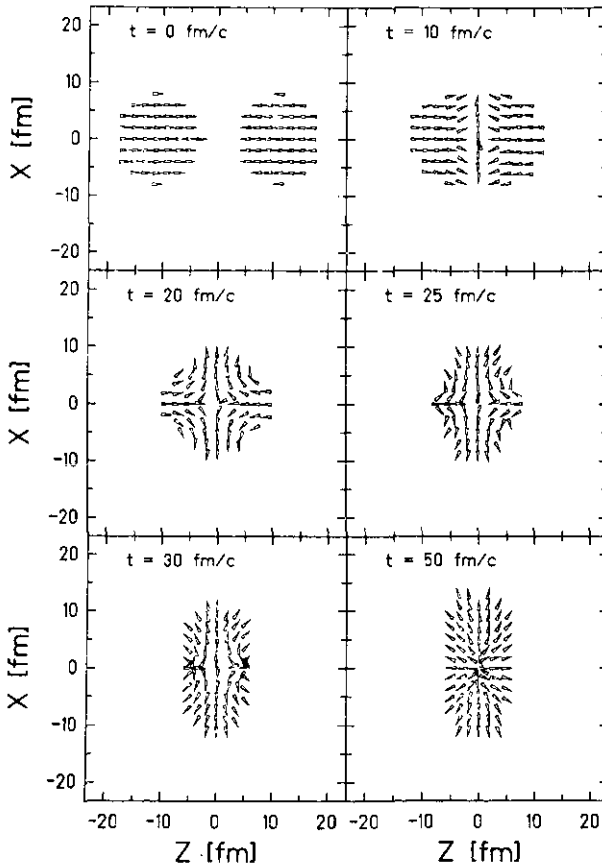

Figure 17. Time evolution of the reaction ^{197}Au (200 MeV/nucleon, $b = 0$ fm) + ^{197}Au in velocity space. Observe the formation of a shock front where the nucleons are deflected to sidewards angles.

First we investigate the evolution of the reaction Au (200 MeV/nucleon, $b = 0$ fm) + Au in velocity space. Figure 17 shows the highly anisotropic initial configuration. When the nuclei start to touch each other in coordinate space the nucleons in the overlap region are deflected to sidewards angles. This is a beautiful microscopic proof of the behaviour predicted by hydrodynamics [1–18], i.e. a zone of shocked matter is formed.

The time evolution of the density along the beam direction (figure 18) reveals this scenario. First a very small high density region is formed in the centre of the reaction. This region then expands due to the further flux of matter from projectile
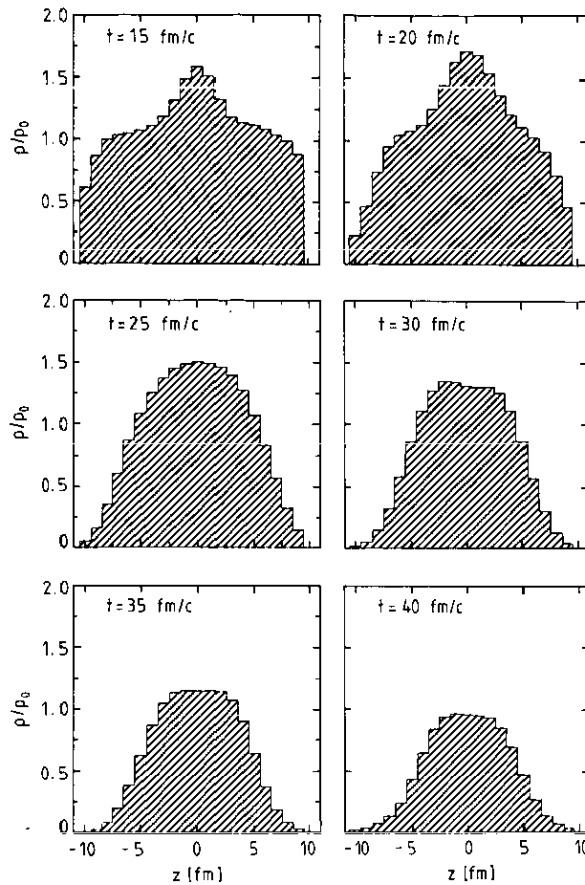
Figure 18. Density profiles along the beam direction for the same reaction as in figure 17. A plateau with approximately 1.5 times normal nuclear matter density is formed.

and target. A plateau with density about 1.5 times normal nuclear matter density is formed. However, we have to clarify whether this zone is equilibrated or not. The local degree of isotropy R is defined as $R = \langle p_T^2 \rangle / 2 \langle p_L^2 \rangle$, where p_T and p_L are taken in the rest frame of the matter element under consideration. Then $R \approx 0$ means total anisotropy which is characteristic for the first stage of a collision in which the two nuclei just touch and no transverse momentum has yet been transferred. An isotropic momentum distribution would lead to $R = 1$. Note, however, that $R = 1$ is a necessary, but not necessarily sufficient condition for equilibration.

For heavy systems one expects to be close to a local equilibrium situation, where viscous hydrodynamics is applicable. The values of $R(x, z)$ in the reaction plane (x, z) are shown in figure 19. The two nuclei are totally thermalized $(R = 1)$ initially in their respective rest frames. Early in the reaction the interpenetrating nuclei yield a strong anisotropy in this overlap region. The remaining parts of the projectile and target remain equilibrated. At the time of full overlap the central density and temperatures have reached their maximal values. Here $R \approx 0.5$ still appears to be small. When the matter starts to decompress near equilibrium is observed in this central zone.
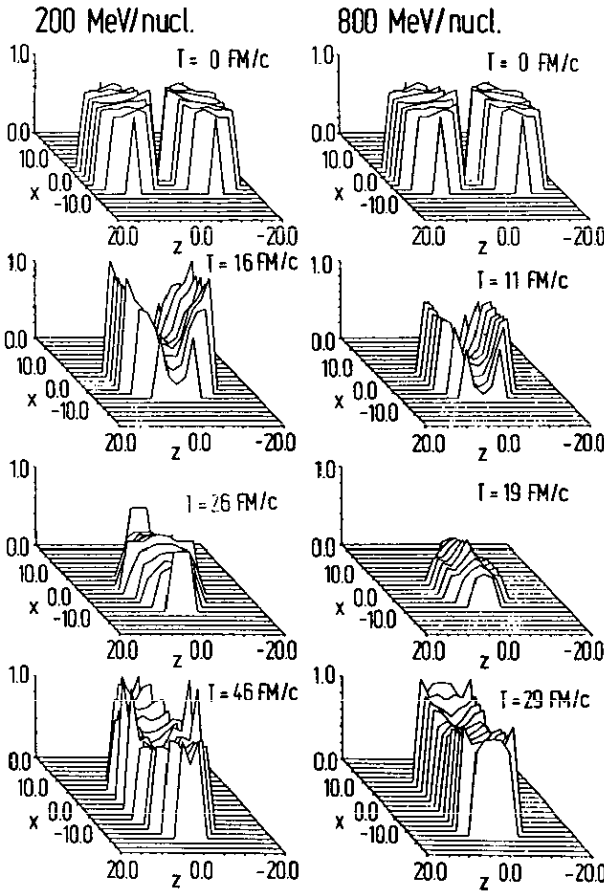
Figure 19. Snapshots of the time evolution of the thermalization ratio $R = \langle P_\perp^2 \rangle / (2 \langle P_\parallel^2 \rangle)$ over the reaction plane in very central collisions. A density cut has been introduced in order to avoid strong statistical fluctuations ($\rho > 0.1 \rho_0$). Equilibration is observed at the end of the reaction in the central zone.

Figure 20 shows the time evolution of R at the origin ($x = y = z = 0$) for the reaction Au ($b = 0$ fm) + Au at 200 and 800 MeV/nucleon bombarding energy. The display is for three different cases, showing R for all nucleons (full curve), for those nucleons which have suffered at least one (broken curve) or even two (dotted curve) collisions. Local equilibrium is clearly *not* achieved for the total system, while the participant component equilibrates better ($R \approx 0.8$–0.9).

4.2. The evaluation of the stress tensor: pressure and viscosity

Information about the thermalization process can also be obtained from the stress tensor

$$P_{kl}(\boldsymbol{r}, t) = \int \mathrm{d}^3 p \, f(\boldsymbol{p}, \boldsymbol{r}, t)(p_k - \langle p_k(\boldsymbol{r}, t) \rangle)(v_l - \langle v_l(\boldsymbol{r}, t) \rangle) \qquad k, l = 1, 3. \quad (9)$$

The interaction part of P_{ik} has been excluded from the analysis, because P_{ik} is to be compared with the Newtonian ansatz used in viscous fluid dynamics [6, 8, 10,
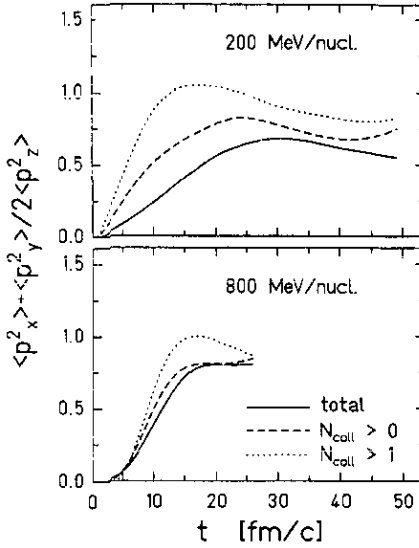
Figure 20. Ratio of the mean quadratic momenta at the origin of the CM frame in the transverse and longitudinal directions for central Au + Au collisions at 200 MeV/nucleon (top) and 800 MeV/nucleon (bottom) for all particles (full curves), for particles which have collide at least once (broken curves) and more than once (dotted curves). The participant component equilibrates much better than the spectators. This behaviour is more pronounced at lower energies.
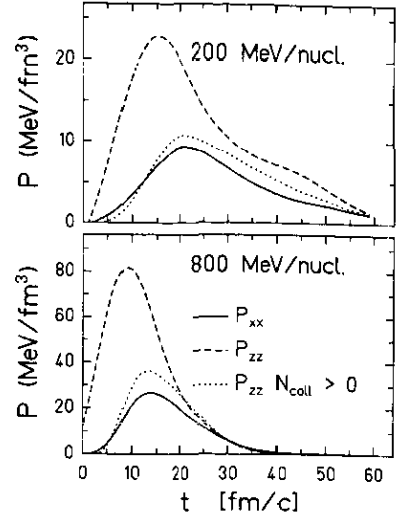
Figure 21. Time dependence of the kinetic pressure in the centre of the reaction for the system Au (200 (top), 800 (bottom) MeV/nucleon, $b = 0$ fm) + Au. The broken curves correspond to the xx and yy components of the stress tensor, full curves to the zz component. A thermal (chain curves) and a non-thermal part (dotted curves) are defined for nucleons which have suffered at least one collision.

76]. For the local interactions used here P_{ik} is trivially isotropic. That means the sum of the kinetic and interaction pressure will always appear to be more isotropic than the kinetic pressure (stress tensor) alone. From the QMD distribution function (see equation (2)) one obtains

$$P_{kl}(\boldsymbol{r}, t) = \frac{1}{(2\pi L)^{3/2}} \sum_{i=1}^{N} \exp\left\{-\frac{(\boldsymbol{r} - \boldsymbol{r}_{i0}(t))^2}{2L}\right\}$$

$$\times (p_{i0} - \langle p(r,t)\rangle)_k ((p_{i0}/m_i) - \langle v(r,t)\rangle)_l. \tag{10}$$

Figure 21 shows the time evolution of the different components of the stress tensor. The maxima of both the zz component (full curve) and the xx component (broken curve) appear at the same time as the maxima of the temperatures and the central densities. However, the absolute values of these components differ from each other, they approach one common value towards the end of the reaction. This again reflects the importance of treating the non-equilibrium aspects during the early course of the reaction.

On the other hand, for fireball nucleons the zz component of the stress tensor (dotted curve) is almost identical to the xx component, i.e. the fireball is near thermal equilibrium.

Hence, the basic assumption of the three-fluid model [9, 15] is justified: each
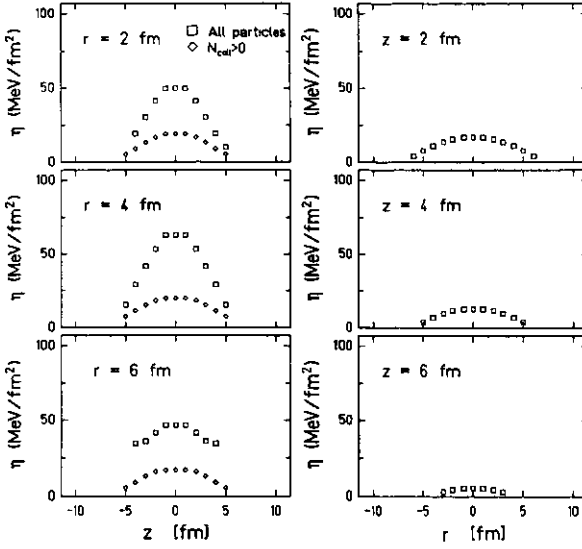
Figure 22. Shear viscosity coefficient η extracted from QMD calculations in the reaction Au (200 MeV/nucleon, $b = 0$ fm) + Au at $t = 20$ fm c^{-1} along the beam direction z (left) and in transverse direction r (right). Note the apparent difference between the viscosity coefficent in the longitudinal and transverse directions.
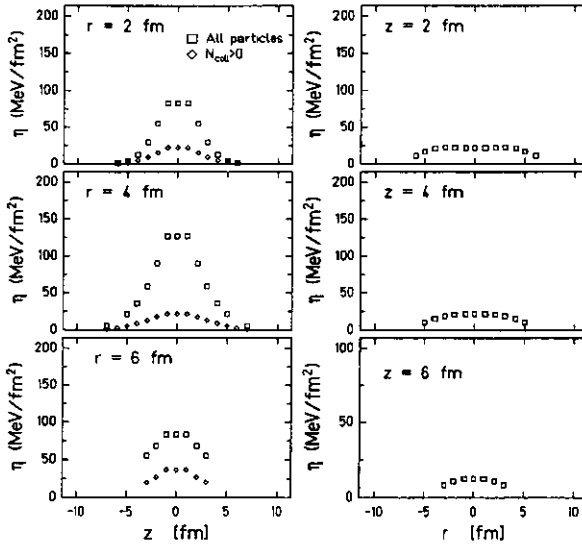

Figure 23. Same as figure 22 for 800 MeV/nucleon (evaluated at 10 fm c^{-1}).

of the three components closely approach thermal equilibrium. The non-equilibrium effects are most important at the beginning of the reaction.

4.3. *The applicability of macroscopic models*

Can the concept of viscous fluid dynamics [6, 8, 10, 76] be applied to heavy ion

collisions? The viscosity coefficients η (shear viscosity) and ξ (bulk viscosity) are defined by the following Newtonian form of the stress tensor.

$$P_{ij} = p \cdot \delta_{ij} - \eta \cdot \left(\frac{\partial V_i}{\partial x_j} + \frac{\partial V_j}{\partial x_i} - \delta_{ij} \frac{2}{3} \cdot \partial V \right) - \delta_{ij} \cdot \zeta \cdot \partial V. \qquad (11)$$

The viscosity and its density and temperature dependence serve as a constitutive equation for hydrodynamical calculations. In a microscopic model these viscosity coefficients can be determined by comparing the exact pressure tensor (equation (9)) to the Newtonian form (equation (11)) [80]. Furthermore this Newtonian ansatz itself can be checked. This means that unique coefficients η and ξ should be found so that all, in general anisotropic, components of the stress tensor obey relation (11) with the *same* coefficients. However, we find here that the coefficients for the longitudinal components of the stress tensor are about a factor of three larger than the coefficient for the transverse component.

Figure 21 shows the shear viscosity coefficient as a function of both the transverse (denoted by r), and the longitudinal (denoted with z) distance from the origin, extracted for the reaction Au (200 MeV/nucleon, $b = 0$ fm) + Au, at 20 fm c^{-1} (note the cylindrical symmetry of the system). The left-hand column shows the longitudinal viscosity coefficient η_{rz} for all particles and for particles which have collided at least once. η_{rz} reaches maximum values around 60 MeV fm^{-2} c^{-1} in the highest density region, if all particles are considered. It drops to zero at larger distances from the centre due to the density and temperature dependence. In contrast, the participant component reaches values of approximately 20 MeV fm^{-2} c^{-1} only. The right-hand column shows the transverse component η_{xy}, which reaches maximum values of 20 MeV fm^{-2} c^{-1}, which are nearly identical to the 'participant' component. The same situation is found for higher energies (see figure 23). A maximum viscosity coefficient of 130 MeV fm^{-2} c^{-1} is needed in order to get a proportionality between the stress tensor and velocity gradient at 800 MeV/nucleon. For the transverse component a maximum value of 20 MeV fm^{-2} c^{-1} is found. A higher value of the viscosity coefficient is found in the longitudinal direction.

Previous one- [6], two- [8] and three-dimensional [10] viscous hydrodynamical calculations used much smaller viscosity coefficients than those obtained by kinetic theories. These low values were motivated by fission fragment spectra, calculated by Hofmann and Nix [81]. However, recently hot fission experiments have lead to much higher extracted viscosity coefficients [82] in accordance with the estimates of kinetic theories [72, 73].

Recent hydrodynamical calculations [76] show that only such high viscosity coefficients can explain the flow and bounce-off data. However, viscosity coefficients of 60 MeV fm^{-2} c^{-1} yield better agreement with the experimentally observed in-plane sidewards, while the off-plane squeeze-out are to be reproduced with $\eta = 40$ MeV fm^{-2} c^{-1} (see also [63]). This is in qualitative agreement with the previous results.

5. Summary and conclusions

We have investigated the 'stopping power' of nuclei and the thermalization process employing the QMD approach.

The mean free path of the nucleons, λ, which has been calculated microscopically, is found to be mass independent, e.g. it can be considered as a 'material' constant. λ, however, is strongly energy dependent; it decreases with the energy, in contrast to the naive expectation based on classical kinetic theory [75], which yields an increasing λ because σ decreases with energy. This decrease is a genuine quantum statistical effect. In the QMD (and the VUU) model it originates from the 'Pauli blocking' of the collisions, which becomes more important at low energies, due to the occupied phase space. The 'soft' collisions at very low $\sqrt{s}$ are found to be most strongly blocked. Even at high energies (1 GeV/nucleon) more than 20% of the collisions are still blocked. Classical molecular dynamics [40–49], which do not include this quantum effect, therefore overestimate stopping, thermalization and collective flow.

The rapidity distributions only show stopping for heavy systems, independent of the energy. However if one takes only free protons and in addition the efficiency filter of the plastic ball into account, the shapes of the dN/dY distributions are also found to be mass independent. The rapidity distributions are very sensitive to the n–n cross sections, but do not depend on the EOS.

In order to analyse the thermalization achieved in heavy ion collisions, a local analysis of macroscopic quantities, such as density, mean moments of the momenta and the pressure, have been performed. We have found that non-equilibrium aspects play an important role in heavy ion reactions. At the time when all the observables from which one wants to extract the equation of state are established, the reaction cannot be cast in a one- or two-fluid dynamical picture. A rapid approach to local equilibration is observed in a three-fluid decomposition. These components can be experimentally distinguished by their clear separation in phase space (Y and p_T). The dynamical evolution of the reaction is dominated by the interaction of the projectile with the participants, and, separately, by the target with the participants. The direct interpenetration of projectile and target is not observed.

The viscous three-component fluid dynamical model and anisotropic hydrodynamics [88] seem to be the only macroscopic models which can incorporate the non-equilibrium effects in a proper way.

This also points to the necessity of looking for signatures of the equation of state in those observables which are dominated by nucleons from the participant component only, because here the distortion of the observables due to 'spectators' and due to momentum-dependent effects is minimized.

References

[1] Scheid W, Müller H and W Greiner 1974 *Phys. Rev. Lett.* **32** 741
[2] Baumgardt H G, Schott J V, Sakamoto Y, Schopper E, Stöcker H, Hofmann J, Scheid W and Greiner W 1975 *Z. Phys.* A **273** 359
[3] Amsden A A, Harlow F H and Nix J R 1977 *Phys. Rev.* C **15** 2059
Amsden A A, Ginocchio J N, Harlow F H, Nix J R, Danos M, Halbert E C and Smith R K 1977 *Phys. Rev. Lett.* **38** 1055
[4] Amsden A A, Goldhaber A S, Harlow F H and Nix J R 1978 *Phys. Rev.* C **17** 2080
[5] Stöcker H, Maruhn J A and Greiner W 1980 *Phys. Rev. Lett.* **44** 725; 1979 *Z. Phys.* A **290** 297
[6] Csernai L P, Lukacs B and Zimanyi J 1980 *Nuovo Cimento Lett.* **27** 111
Csernai L P and Barz H W 1981 *Z. Phys.* A **296** 173
[7] Stöcker H, Csernai L P, Graebner G, Buchwald G, Kruse H, Cusson R Y, Maruhn J A and Greiner W 1981 *Phys. Rev. Lett.* **47** 1807; 1982 *Phys. Rev.* C **25** 1873
[8] Buchwald G, Csernai L P, Maruhn J A, Greiner W and Stöcker H 1981 *Phys. Rev.* **24** 135

[9] Csernai L P, Lovas I, Maruhn J A, Rosenhauer A, Zimanyi J and Greiner W 1982 *Phys. Rev.* C **26** 149

[10] Buchwald G, Graebner G, Theis J, Maruhn J A, Greiner W and Stöcker H 1983 *Phys. Rev.* C **28** 1119

[11] Russkikh 1983 *Sov. J. Nucl. Phys.* **38** 381; 1986 *Sov. J. Nucl. Phys.* **44** 961

[12] Buchwald G, Gräbner G, Theis J, Maruhn , W. Greiner W and Stöcker H 1984 *Phys. Rev. Lett.* **52** 1594

[13] Ivanov Y B and Satarov L M 1985 *Nucl. Phys.* A **433** 713

[14] Clare R B and Strottman D 1986 *Phys. Rep.* **141** 172

[15] Rosenhauer A, Maruhn J A, Greiner W and Csernai L P 1987 *Z. Phys.* A **326** 213

[16] Mishustin I N 1989 *Nucl. Phys.* A **494** 595

[17] Satarov L M 1990 *Sov. J. Nucl. Phys.* **52** 264

[18] Stöcker H and Greiner W 1986 *Phys. Rep.* **137**

[19] Gustafsson H A *et al* 1984 *Phys. Rev. Lett.* **52** 1590

[20] Renfordt R E 1984 *Phys. Rev. Lett.* **53** 763

[21] Beauvis D 1983 *Phys. Rev.* C **27** 2443

[22] Ritter H G *et al* 1985 *Nucl. Phys.* A **447** 3c

[23] Doss K G B *et al* 1986 *Phys. Rev. Lett.* **57** 302

[24] Doss K G B *et al* 1987 *Phys. Rev. Lett.* **59** 2720

[25] Jacak B V *et al* 1987 *Phys. Rev.* C **35** 1751

[26] Kampert K H 1989 *J. Phys. G: Nucl. Part. Phys.* **15** 691–740

[27] Gutbrod H H, Poskanzer A M and Ritter H G 1989 *Rep. Prog. Phys.* **52** 1267

[28] Gutbrod H H, Kampert K H, Kolb B W, Poskanzer A M, Ritter H G and Schmidt H R 1990 *Z. Phys.* A **337** 57–69

[29] Schmidt H R *GSI Report* 91–03

[30] Kruse H, Jacak B V and Stöcker H 1985 *Phys. Rev. Lett.* **54** 289

[31] Molitoris J J and Stöcker H 1985 *Phys. Rev.* C **32** 346; 1985 *Phys. Lett.* **162B** 47

[32] Kruse H, Jacak B V, Molitoris J J, Westfall G D and Stöcker H 1985 *Phys. Rev.* C **31** 1770

[33] Molitoris J J, Stöcker H and Winer B L 1987 *Phys. Rev.* C **36** 220

[34] Gregoire C, Remaud B, Sebille F and Vinet L 1987 *Nucl. Phys.* A **465** 317

[35] Bertsch G F, Kruse H and Das Gupta S 1984 *Phys. Rev.* C **29** 673

[36] Aichelin J and Stöcker H 1985 *Phys. Lett.* **163** 59

[37] Aichelin J and Bertsch G F 1985 *Phys. Rev.* C **31** 1730

[38] Gale C, Bertsch G F and Das Gupta S 1987 *Phys. Rev.* C **35** 1666

[39] Bertsch G F, Lynch W G and Tsang M B 1987 *Phys. Lett.* **189B** 384

[40] Bodmer A and Panos C N 1977 *Phys. Rev.* C **15** 1342

[41] Wilets L, Henley E M, Kraft M and Mackellar A D 1987 *Nucl. Phys.* A **282** 341

[42] Wilets L, Yariv Y and Chestnut R 1978 *Nucl. Phys.* A **301** 359

[43] Callaway D J E, Wilets L and Yariv Y 1979 *Nucl. Phys.* A **327** 250

[44] Bodmer A R, Panos C, MacKellar A D 1980 *Phys. Rev.* C **22** 1025

[45] Molitoris J J, Hoffer J B, Kruse and Stöcker H 1984 *Phys. Rev. Lett.* **53** 899

[46] Kiselev S M and Pokroskil Yu E 1983 *Sov. J. Nucl. Phys.* **38** 46

[47] Kiselev S M 1984 *Sov. J. Nucl. Phys.* **39** 18

[48] Kiselev S M 1986 *Sov. J. Nucl. Phys.* **44** 610

[49] Schlagel T J and Pandharipande V R 1987 *Phys. Rev.* C **36** 192

[50] Aichelin J and Stöcker H 1986 *Phys. Lett.* **176A** 14

[51] Peilert G, Rosenhauer A, Aichelin J, Stöcker H and Greiner W 1988 *Mod. Phys. Lett.* A **3** 459; 1989 *Phys. Rev.* C **39** 1402

[52] Aichelin J, Peilert G, Bohnet A, Rosenhauer A, Stöcker H and Greiner W 1988 *Phys. Rev.* C **37** 2451

[53] Aichelin J 1991 *Phys. Rep.* **202** 233

[54] Berenguer M, Hartnack C, Peilert G, Rosenhauer A, Schmidt W, Aichelin J, Maruhn J A, Greiner W and Stöcker H 1989 *Proc. Winter School on Nuclear Physics (Les Houches, France)*

[55] Hartnack C 1989 *Diploma Thesis* Universität, Frankfurt unpublished

[56] Beauvais G E, Boal D H and Wong J C K 1987 *Phys. Rev.* C **36** 192

[57] Boal D H and Glosli J M 1988 *Phys. Rev.* C **38** 1870; 1987 *Phys. Rev.* C **38** 2621

[58] Boal D H, Gosli J H and Wicentowich C 1989 *Phys. Rev.* C **40** 601

[59] Botermans W and Malfliet R 1986 *Phys. Lett.* **171B** 22

[60] ter Haar B, Malfliet R and Botermans W 1986 *Phys. Lett.* **172B** 10; 1987 *Phys. Rep.* **149** 207
[61] Cugnon J, Lejeune A and Grange P 1987 *Phys. Rev.* C **35** 861
[62] Ohtsuka N, Linden R, Faessler A and Malik F B 1987 *Nucl. Phys.* A **465** 550
[63] Ainsworth T L, Baron E, Brown G E, Cooperstein J and Prakash M 1987 *Nucl. Phys.* A **464** 740
[64] Schürmann B 1988 *Mod. Phys. Lett.* A **12** 1137
[65] Schürmann B and Zwermann W 1987 *Phys. Rev. Lett.* **59** 2848
[66] Cusson R Y, Reinhardt P G, Molitoris J J, Stöcker H, Strayer M, Greiner W 1985 *Phys. Rev. Lett.* **55** 2786
[67] Keane D, Chu S Y, Fung S Y, Liu Y N, Qiao L J, VanDalen G, Vient M, Wang S, Molitoris J J and Stöcker H 1987 *Proc. VIIIth High Energy Heavy Ion Study (LBL Berkeley)*; 1988 *Phys. Rev.* C **37** 1447
[68] Ayik S and Gregoire C 1988 *Phys. Lett.* **212B** 269; 1990 *Nucl. Phys.* A **513** 187
[69] Randrup J and Remaud B 1990 *Nucl. Phys.* A **514** 339
[70] Feldmeier H 1990 *Nucl. Phys.* A **515** 147
[71] Dorso C, Duarte S and Randrup J 1987 *Phys. Lett.* **188B** 287
[72] Peilert G, Randrup J, Stöcker H and Greiner W 1991 *Phys. Lett.* B **260** 271
[73] Bodmer A R 1978 *Proc. Symp. on Relativistic Heavy-Ion Research (GSI Darmstadt)*; *Preprint* Argonne National Laboratory
[74] Danielewicz P 1984 *Phys. Lett.* **146B** 168
[75] Sobel M I, Siemens P J, Bondorf J B and Bethe H A 1975 *Nucl. Phys.* A **251** 502
[76] Schmidt W 1989 *Thesis* Universität Frankfurt; 1989 *GSI Report* 89-16; 1989 *Proc. NATO Advanced Study Institute on the Nuclear Equation of State (Peniscola, Spain, 1989): Part A: Discovery of Nuclear Shockwaves and the EOS (NATO ASI Series, Series B: Physics 216A)* ed W Greiner and H Stöcker p 197
[77] Uehling E A and Uhlenbeck G E 1933 *Phys. Rev.* **43** 552; 1979 *Phys. Rev.* **46** 917
[78] Randrup J 1979 *Nucl. Phys.* A **314** 429
[79] Cugnon J, Mitzutani T and Vermeulen J 1981 *Nucl. Phys.* A **352** 505
[80] Rosenhauer A, Csernai L P, Maruhn J A, Greiner W 1984 *Phys. Scr.* **30** 45
[81] Cugnon J and Hote D L 1984 *Proc. 7th High Energy Heavy Ion Study, GSI Darmstadt (GSI Report 85)* p 253
[82] Hofmann H and Nix J R 1983 *Phys. Lett.* **122B** 117
[83] Paul P private communication; *Preprint* State University of Stony Brook
[84] Sorge H, Stöcker H and Greiner W 1989 *Ann. Phys., NY* **192** 266
[85] von Keitz A, Winckelmann L, Jahns A, Sorge H, Stöcker H and Greiner W 1991 *Preprint* University of Frankfurt, UFTP 255; 1992 *Phys. Lett.* B submitted
[86] Bloomer M 1990 *Thesis* MIT
[87] Wenig S 1990 *Thesis* Universität of Frankfurt
[88] Neise L W 1990 *Thesis* University of Frankfurt; *GSI Report* 90-24